chemosensors

MDPI

Article

Electrochemical Biosensor Employing Bi_2S_3 Nanocrystals-Modified Electrode for Bladder Cancer Biomarker Detection

Yunong Zhao [1,†], Yanbing Tao [1,†], Qing Huang [1], Jing Huang [1], Jiayu Kuang [1], Ruiqin Gu [1], Pei Zeng [2], Hua-Yao Li [1], Huageng Liang [2] and Huan Liu [1,*]

[1] School of Optical and Electronic Information, Wuhan National Laboratory for Optoelectronics, Optics Valley Laboratory, Huazhong University of Science and Technology, Wuhan 430074, China; zyn248@hust.edu.cn (Y.Z.); taoyanbing@hust.edu.cn (Y.T.); 2021511006@hust.edu.cn (Q.H.); m202172736@hust.edu.cn (J.H.); kuangjy@hust.edu.cn (J.K.); d201780593@hust.edu.cn (R.G.); huayaoli@hust.edu.cn (H.-Y.L.)

[2] Department of Urology, Union Hospital, Tongji Medical College, Huazhong University of Science and Technology, Wuhan 430022, China; m202075934@hust.edu.cn (P.Z.); leonard19800318@hust.edu.cn (H.L.)

* Correspondence: huan@hust.edu.cn

† These authors contributed equally to this work.

Abstract: Bladder cancer is a kind of malignant tumor with high incidence in the urinary system, complex pathogenic causes, and the high recurrence rate. Biosensors capable of rapid, on site, and accurate bladder cancer diagnosis method continue to be lacking. Here, the electrochemical biosensor for detecting cytokeratin 18 (CK18, bladder cancer biomarker) was constructed based on the chemically modified electrode (CME). The work electrode (WE) was modified by bismuth sulfide semiconductor nanocrystals (Bi_2S_3 NCs), and then immobilized with CK18 antibodies and blocking agents to complete the electrode preparation. The results indicated that the interface of a flexible carbon electrode with Bi_2S_3 NCs film was steady with reliable charge transfer capability. With the large specific area and quantum size effect, the proposed sensor could detect CK18 antigen protein with an ultralow detection limit of 1.87 fM (fmol L^{-1}) and wide linear dynamic range of 1–1000 pg mL^{-1}, respectively. Detecting results could be read in less than 30 s with the portable, planar flexible CME. The sensitive and specific electrochemical biosensor possessed the characteristics of rapidity, ease-of-use, and non-invasive detection, indicating the application prospect in the early screening of bladder cancer and other diseases.

Keywords: electrochemical biosensor; bismuth sulfide nanocrystals; chemically modified electrode; bladder cancer; biomarker detection; cytokeratin 18 protein

check for updates

Citation: Zhao, Y.; Tao, Y.; Huang, Q.; Huang, J.; Kuang, J.; Gu, R.; Zeng, P.; Li, H.-Y.; Liang, H.; Liu, H. Electrochemical Biosensor Employing Bi_2S_3 Nanocrystals-Modified Electrode for Bladder Cancer Biomarker Detection. *Chemosensors* **2022**, *10*, 48. https://doi.org/10.3390/chemosensors10020048

Academic Editors: Dan Xie, Jian-Long Xu, Yilin Sun and Boris Lakard

Received: 22 December 2021
Accepted: 25 January 2022
Published: 27 January 2022

Publisher's Note: MDPI stays neutral with regard to jurisdictional claims in published maps and institutional affiliations.

Copyright: © 2022 by the authors. Licensee MDPI, Basel, Switzerland. This article is an open access article distributed under the terms and conditions of the Creative Commons Attribution (CC BY) license (https://creativecommons.org/licenses/by/4.0/).

1. Introduction

Bladder cancer is one of the most common malignant tumors of the urinary system, and the incidence ranks ninth among all malignant tumors [1]. Owing to the complex and unclear pathogenic causes and high recurrence rate, bladder cancer is usually diagnosed in the middle and advanced stages of the cancer, bringing great physical and mental harm to patients [2]. The diagnostic methods of bladder cancer mainly include cystoscopy, tissue biopsy, in vitro imaging, and liquid biopsy [3]. Cystoscopy and tissue biopsy are used extensively as the gold standard in the diagnosis of bladder cancer. Cystoscopy has been improved recently; problems including hematuria or urethral pain may occur within a few days after the detection, causing the limited diagnosis effect of early bladder cancer [4,5]. Tissue biopsy can analyze the morphology of bladder cancer cells invasively with certain specificity and sensitivity, which usually take multiple sample processing steps. Although in vitro imaging technology is not invasive, it has a high false-positive rate in the early diagnosis of cancer, which affects the diagnosis. There is a critical need for rapid, accurate,

and non-invasive diagnostic methods for bladder cancer, to promote early screening and long-term monitoring.

Liquid biopsy, as a non-invasive detection method, mainly detects biomarkers in body fluids or secretions through optical, electrochemical, magnetism, and immunology principle, which reflects the expression of tumor cells [6–8]. Since tumor molecular abnormalities in body fluid are usually earlier than structural imaging abnormalities, and bladder tumors are in direct contact with urine, liquid biopsy of tumor markers in urine is a promising diagnostic method for bladder cancer [9–11]. Biomarkers of bladder cancer mainly include DNA, mRNA, protein, and cells. Cytokeratin (CKs) and nuclear matrix protein (NMP) are key biomarkers of urogenital lesions in the diagnostic and prognostic stage [12]. The occurrence of tumors would lead to the changes in the content of metabolites [13]. Numerous studies have suggested that the content of NMP22, CK7, CK18, CK19, CK20, and other cytokeratin are closely related to bladder cancer [14,15]. Low-concentration and accurate detection of bladder cancer biomarkers could enhance the effect of early diagnosis, therapeutic efficacy observation, and recurrence monitoring. Immunoassay-based techniques including electrochemiluminescence (ECL) immunoassay, enzyme-linked immunosorbent assay (ELISA) and gold immunochromatography assay (GICA) are the most commonly used methods to detect CKs biomarkers [16]. The above techniques generally require multiple preparation and processing steps, and the support of sophisticated instruments. Hence, the synergetic improvement of detection speed and accuracy needs to be given higher priority.

Biosensors enable a combination of bioactive materials and a corresponding transducer for the determination of a specific chemical or biological substance, mainly including electrical types and optical types. The optical biosensors based on fluorescence spectroscopy, surface plasmon resonance (SPR), dynamic light scattering (DLS), and Raman scattering (RS) have been utilized for the detection of bladder cancer biomarkers [17–19]. The above methods usually require multiple sample preparation or processing steps, and still depend on sophisticated instrument for measurement, restricting the field application. The most essential advantage of biosensor is the fact that it could realize rapid, low-cost, and convenient sensing and detection, which is suitable for clinical lab and point-of-care testing (POCT), as well as a home-use test [20]. The chemically modified electrode (CME) utilized in the design of electrochemical devices and systems has been proved to be a kind of promising biosensor for the detection of biologically active molecules [21]. A typical CME consists of a three-electrode structure, namely, a reference electrode (RE), a counter electrode (CE), and a working electrode (WE). As a mature commercial CME, glucose test strip is of high reference value. Conductor or semiconductor WEs are coated with well-explored modified materials (monomolecular, multi-molecular, ionic, or polymer), and the electrochemical properties of the modified films are presented through Faraday reactions [22]. CMEs for antigen-antibody detection faces the first issue of signal transduction of biochemical reaction. Yang, et al. [23] constructed MoS_2 nanosheet field-effect transistor (FET) sensor arrays for the detection of nuclear matrix protein 22 (NMP22) and cytokeratin 8 (CK8) with linear detection range of 10^{-6} to 10^{-1} pg mL^{-1} and the limit of detection (LOD) of 0.027 and 0.019 amol L^{-1} (10^{-18} mol L^{-1}), respectively.

High-efficiency enrichment and stable adhesion of biomarker proteins on the surface of the electrode favor the sensitive and specific protein detection. Compared with bulk materials, semiconductor nanocrystals (NCs) possess a larger specific surface area, and high surface activity, enabling their sufficient adsorption and stable presence on protein surface [24]. The physicochemical properties, and sensitive effects of NCs could be regulated by controlled synthesis, surface modification and interfacial engineering for specific biological proteins [25]. It is remarkable that the suitable binding or anchoring of different biological protein molecules could be achieved by tunable size and functional groups on the surface, which makes it possible to combine with proteins and peptides, leading to meliorative specific labeling activity [26]. Almost uniquely, the quantum effect (coulomb blockade effect and quantum tunneling effect) of NCs may yield interesting effects in the

signal transduction of antigen-antibody binding reactions [27]. Moreover, semiconductor NCs can be solution-processed at room temperature onto a wide variety of substrates, including flexible and rigid substrates, so that their material properties are well preserved in real devices. Photoluminescence (PL), including the fluorescence and phosphorescence processes, are the optical phenomena that semiconductor gives light emission through absorbing incident light whose energy is higher than the energy band gap of the semiconductor. The excited electrons generated via the optical excitation would return to the ground state, accompanied by the emitting of the photons. The fluorescence detection based on NCs mainly depends on the optical properties change of NCs including fluorescence intensity, spectral position and shape, excited state lifetime, or fluorescence polarization due to the interaction between the fluorescent material and the analyte. Through the fluorescence quenching process of donor-acceptor electron transfer (or energy transfer), the specific binding reaction of antigen and antibody can be transduced into the optical signal. Bismuth sulfide (Bi_2S_3), as a green and non-toxic semiconductor material, has been widely used in the field of sensing, biological detection, and medical imaging [28]. It is worth noting that the usage of semiconductor NCs in electrochemical biosensing may be an effective strategy.

In this paper, environmentally friendly bismuth sulfide nanocrystals (Bi_2S_3 NCs) were prepared by a hydrothermal method. For the detection of bladder cancer biomarker CK18, a planar chemically modified electrode was prepared using Bi_2S_3 NCs as modification material. Specific binding reaction of CK18 antigen and antibody was transduced to the electrical signal of the biosensor employing Bi_2S_3 NCs-modified electrode. The developed all-solid-state electrochemical biosensor exhibits the characteristics of rapid detection (less than 30 s), high sensitivity (LOD of 1.87 fM [fmol L^{-1}]), and wide linear dynamic range (1–1000 pg mL^{-1}) for bladder cancer biomarker detection, which is expected to be applied in the field of medical Lab, POCT, wearable health monitoring, and community health screening.

2. Materials and Methods

2.1. Reagents

Ammonium bismuth citrate ($Bi[NH_3]_2C_6H_7O_7{\cdot}H_2O$) (purity: 99%) and thioacetamide (CH_3CSNH_2) (purity: 99%) were acquired from Beijing InnoChem Science & Technology Co., Ltd. (Beijing, China). Phosphate buffered saline (PBS, 0.067 M) was purchased from GE Healthcare Life Sciences Hyclone Laboratories (Logan, UT, USA.). Bovine Serum Albumin (BSA) (purity: 99.5%) was provided by Shanghai Aladdin Biochemical Technology Co., Ltd. (Shanghai, China). Recombinant human cytokeratin 18 protein (CK18 antigen) (purity: >90%, 0.5 mg mL^{-1}) and anti-cytokeratin 18 antibody (CK18 antibody) (purity: tissue culture supernatant, 1 mg mL^{-1}) were obtained from Abcam plc. (Cambridge, UK).

2.2. Instruments

X-ray diffraction (XRD) measurements were obtained using a diffractometer (D/MAX 2500V, Rigaku, Tokyo, Japan). The transmission electron microscope (TEM) characterization was obtained using a Titan G2 60-300 transmission electron microscope (FEI, Eindhoven, Netherlands). The scanning electron microscope (SEM) images were acquired by GeminiSEM300 scanning electron microscope (Carl Zeiss, Oberkochen, Germany). Fourier transform infrared spectra (FTIR) were acquired by VERTEX 70 infrared spectrometer (Bruker, Karlsruhe, Germany).

2.3. Synthesis of Bi_2S_3 Nanocrystals

Bismuth sulfide nanocrystals (Bi_2S_3 NCs) were prepared by the mild hydrothermal method. Ammonium bismuth citrate ($Bi[NH_3]_2C_6H_7O_7{\cdot}H_2O$) aqueous solution (0.005 M) and thioacetamide (CH_3CSNH_2) aqueous solution (0.0075 M) were used as bismuth source and sulfur source, respectively. A total of 30 mL ammonium bismuth citrate aqueous solution was added to the three-neck flask and stirred at 90 °C for 10 min, while the

thioacetamide aqueous solution was placed at the atmosphere of 90 °C. The above sulfur source was slowly added into the three-neck flask and reacted at 90 °C for 2 h to prepare Bi_2S_3 NCs. The reaction product was washed by deionized water and anhydrous ethanol for 3–5 times, and purified samples were obtained and dispersed in anhydrous ethanol (10 mg mL^{-1}).

2.4. Fabrication of Bi_2S_3 NCs-Modified Electrode

The planar electrochemical electrode was obtained from Qingdao Poten Technology Co., Ltd. (Qingdao, China). The dimensions of the electrode body are 32 mm × 12 mm × 0.3 mm (length × width × height). The working electrode (WE) and counter electrode (CE), and the reference electrode (RE) are made of carbon and silver/silver chloride (0.5 M KCl), respectively. The electrode substrate is made of polyethylene terephthalate (PET). The Bi_2S_3 NCs were dissolved in ethanol to prepare 10 mg mL^{-1} NCs solutions for sensor fabrication. Next, 1 µL Bi_2S_3 solution was dripped onto carbon electrode, which was dip-coated at room temperature. The above step was repeated three times to form NC films. After drying at room temperature for 10 min, the Bi_2S_3 NCs-modified electrode (C/Bi_2S_3) was prepared. NCs-modified electrode was incubated in CK18 antibody solution at 37 °C for 1 h (C/Bi_2S_3/Antibody), then washed with PBS solution and dried at room temperature. Subsequently, the antibody-coated NCs-modified electrode was incubated in BSA solution (10 mg mL^{-1}) for 2 h, then washed by PBS and dried at room temperature to prepare the final C/Bi_2S_3/Antibody/BSA electrode.

2.5. Electrochemical Characterization

The following electrodes: bare carbon electrode (C), C/Bi_2S_3, C/Bi_2S_3/Antibody, and C/Bi_2S_3/Antibody/BSA were tested in PBS containing 5 mM $(Fe[CN]_6)^{3-/4-}$ and 0.5 M KCl as REDOX mediator by cyclic voltammetry (CV), differential pulse voltammetry (DPV), and electrochemical impedance spectroscopy (EIS). After adding PBS solution on the surface of the C/Bi_2S_3/Antibody/BSA electrode, the DPV and EIS measurement was carried out. Then, different concentrations of recombinant human cytokeratin 18 protein (CK18 antigen) were injected into above PBS solution to perform antigen testing. All the electrochemical data were recorded with the WE, the RE, and the CE by the electrochemical workstation (CHI760e, Shanghai, China). The information about the software: CHI Version 14.05 by CH Instruments, Inc. (3700 Tennison Hill Drive Austin, TX, USA).

3. Results

3.1. Electrochemical Characterization of Bi_2S_3 NCs-Modified Electrode

The basic electrochemical characteristics of the modified electrodes were obtained by CV, DPV and EIS utilizing 5 mM $(Fe[CN]_6)^{3-/4-}$ and 0.5 M KCl as REDOX mediator. As shown in Figure S1, the effective surface areas (A_{eff}) of bare and modified sensors were calculated to be 0.134 cm^2 and 0.109 cm^2, which may be ascribed to the better conductivity of carbon conductor electrodes than bismuth sulfide semiconductor nanocrystals [29]. For purpose of comparison, a bare electrode (C), Bi_2S_3 NCs-modified electrode (C/Bi_2S_3), and an antibody-coated NCs-modified electrode before (C/Bi_2S_3/Antibody) and after BSA-blocking (C/Bi_2S_3/Antibody/BSA) were prepared and tested measured in the presence of PBS (0.067 M) containing above REDOX mediator.

According to CV measurement, all above electrodes (C, C/Bi_2S_3, C/Bi_2S_3/Antibody, and C/Bi_2S_3/Antibody/BSA) displayed sensitive and reversible REDOX peaks, manifesting the planar three-electrode system possesses the capability of converting the charge transfer across the electrode interface (Figure 1a). In addition, different functional modification steps would affect the current intensity of these electrodes, indicating the difference of charge transfer ability of different functional modification layers. Compared with the oxidation peak current (116.3 µA) of bare a C electrode, the C/Bi_2S_3 electrode exhibited slightly lower oxidation peak current (82.89 µA), indicating that the charge transfer capability of NCs modified layer was well maintained. As the antibody and BSA protein were

immobilized on the surface of NCs solid films, the change of conduction capabilities could be ignored, but remained stable.

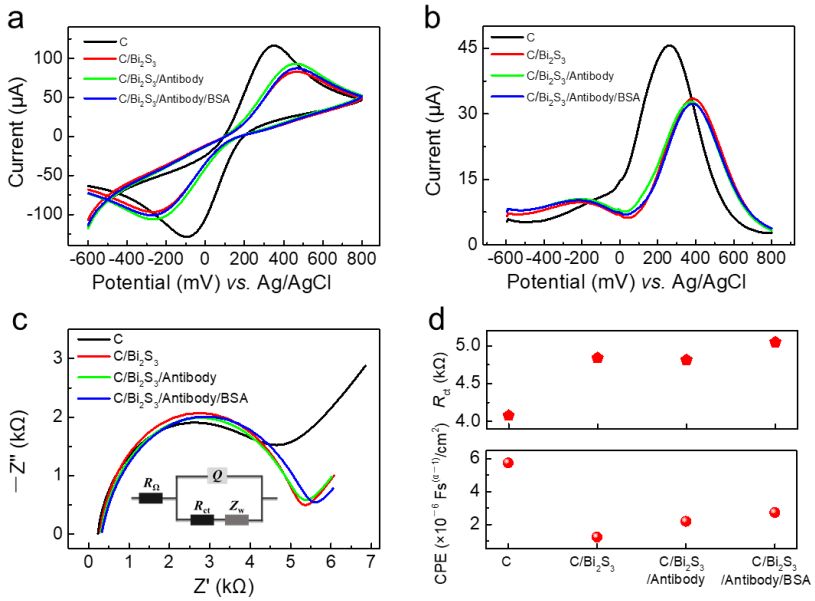

Figure 1. (**a**) CV, (**b**) DPV, and (**c**) EIS characterizations of bare carbon electrode(C), C/Bi_2S_3, C/Bi_2S_3/Antibody, and C/Bi_2S_3/Antibody/BSA in the presence of PBS containing 5 mM $[Fe(CN)_6]^{3-/4-}$ and 0.5 M KCl as REDOX mediator; (**d**) R_{ct} and CPE values of C, C/Bi_2S_3, C/Bi_2S_3/Antibody, and C/Bi_2S_3/Antibody/BSA electrodes.

DPV mode (Figure 1b) can greatly reduce the blank value and ensure high sensitivity and good resolution, which can be used for detection of low concentration biologically active substances. Compared with the oxidation peak current (45.66 μA) of bare carbon electrode (C), C/Bi_2S_3 electrode exhibited slightly lower oxidation peak current (35.14 μA). The peak current decreased from 35.14 μA to 31.3 μA and 29.79 μA for C/Bi_2S_3/Antibody electrode and C/Bi_2S_3/Antibody/BSA electrode, respectively. With the immobilizing of antibody and BSA protein, conduction capability of modified electrodes became slightly worse. The above results demonstrated that NCs modification layer enhanced the charge transfer across the interface from solution to solid electrode.

EIS characterization could give the quantitative parameters of the equivalent circuit model to analyze the electrochemical system and the properties of the electrode process [30]. The inset of Figure 1c displayed the equivalent circuit model of the modified electrode, the current intensity is influenced by Q and R_{ct}, which represents the capacitance of the electrical double layer and the charge transfer resistance of the liquid-solid interface. According to the extraction of R_{ct} from Figure 1c, the NCs modification layer resulted in a slight increase in R_{ct}, perhaps due to the better conductivity of carbon conductor electrodes than semiconductors (Figure 1d). We also concluded that for the electrical double layer, NCs modification layer significantly reduced the value of CPE (constant phase angle element, proportional to C_d). The constant phase element is a capacitive element with a frequency-independent negative phase between current and voltage which interpolates between a capacitor and a resistor. Owing to the poor electrical conductivity of the protein, the R_{ct} value increased gradually with the immobilizing of antibody and BSA. Interestingly, the final C/Bi_2S_3/Antibody/BSA electrode possessed highest R_{ct} and a relatively larger value of CPE among above modified electrodes. These results may explain the unique transduction effect of NCs in the signal transduction of antibody and antigen specific binding reaction.

3.2. Characterization of Bi_2S_3 NCs and Bi_2S_3 NCs-Modified Electrode

The morphology of Bi_2S_3 NCs was characterized through TEM. Figure 2a displays the low magnification TEM image of NCs revealing the uniformly dispersed granular morphology. High resolution TEM analysis further displayed that Bi_2S_3 NCs were nearly spherical nanocrystals with diameter of about 4 nm (Figure 2b). The small size and large specific surface area of NCs are conducive to the enrichment and binding biological proteins. The lattice fringes indicated the lattice spacing of 0.199 nm and 0.357 nm, which respectively corresponded to the (001) and (130) facets of Bi_2S_3, suggestive of the well crystallinity [31]. To further identify the crystal structures of Bi_2S_3 NCs, XRD patterns are displayed in Figure 2c. The two typical diffraction peaks of the NCs powder at approximately 2θ = 20.3° and 25.1° could be observed, which were in good agreement with the (001) and (130) facets clearly observed in HRTEM image [32].

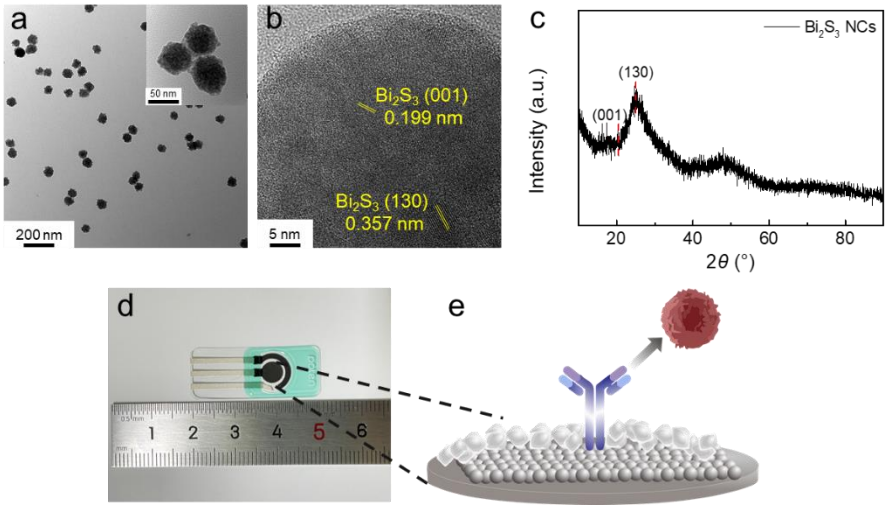

Figure 2. (**a**) TEM images of Bi_2S_3 NCs, and (**b**) HRTEM image of Bi_2S_3 NCs; (**c**) XRD patterns of Bi_2S_3 NCs; (**d**) Optical image of Bi_2S_3 NCs-modified electrode; and (**e**) Schematic diagram of Bi_2S_3 NCs-modified electrode as electrochemical biosensor.

Figure 2d displays the optical image of the planar electrochemical biosensor based on the Bi_2S_3 NCs-modified electrode. Here, CK18 antibodies were modified on the electrode surface to detect CK18 antigen (Figure 2e). More details of the morphology of Bi_2S_3 NCs-modification layer were characterized by SEM. Figure 3a shows that the NCs solid film presented a relatively flat surface with regular gaps and holes dispersed evenly on the electrode surface. After coating with BSA, granular protein molecules appeared on the surface of the NCs solid film, which reduced the quantity of pores and gaps on the electrode surface to a certain extent (Figure 3b). The cross-section SEM image indicated that the NCs film presents the uniformity of thickness (Figure 3c). The cross-sectional element distribution (Figure 3d–f) suggested that the NCs film and NCs-antibody protein interfaces were compact. Energy dispersive spectrometer (EDS) spectra indicated that the bismuth and sulfur elements of NCs were uniformly distributed on the electrode surface (Figure 3d,e). The carbon element was distributed throughout the section due to the carbon electrode and PET substrate (Figure 3f). The universal fabrication processes of all-solid-state planar biosensor are expected to improve the device consistency in large-scale production.

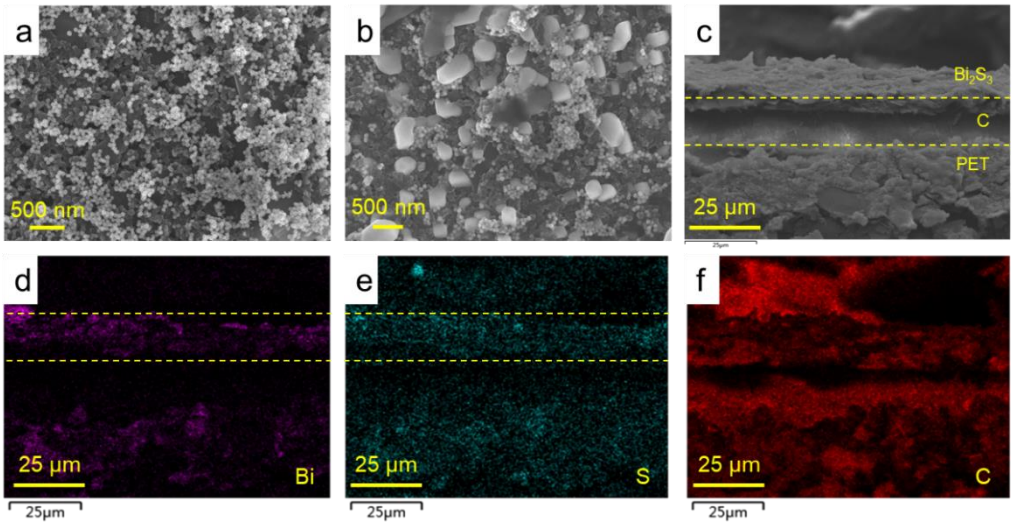

Figure 3. (**a**) SEM image of Bi_2S_3 NCs film on the WE, revealing uniform morphology; (**b**) SEM image of BSA-blocking Bi_2S_3 NCs film on the work electrode; and (**c**) The cross-sectional SEM image of Bi_2S_3 NCs film on the WE. (**d**–**f**) The EDS spectra of cross-sectional Bi_2S_3 NCs film on the WE.

We provide the surface functional groups characterization of different modification layers using Fourier transform infrared spectroscopy (FTIR) (Figure 4). After coating with the antibody, the characteristic peaks of carbonyl derive from the carboxy groups of NCs and the antibody appeared (Figure 4a). After blocking treatment with BSA, the characteristic peak at 1662 cm^{-1} corresponding to the amide of BSA could be observed [33,34], identifying the presence of BSA on the NCs modification layer (Figure 4b). Compared to the antigen-antibody complex, the Bi_2S_3/Antibody/BSA/Antigen sample displayed similar trend of characteristic peaks, suggesting that the antigen-antibody specific binding reaction could proceed normally on the surface of Bi_2S_3 NCs-modified electrode.

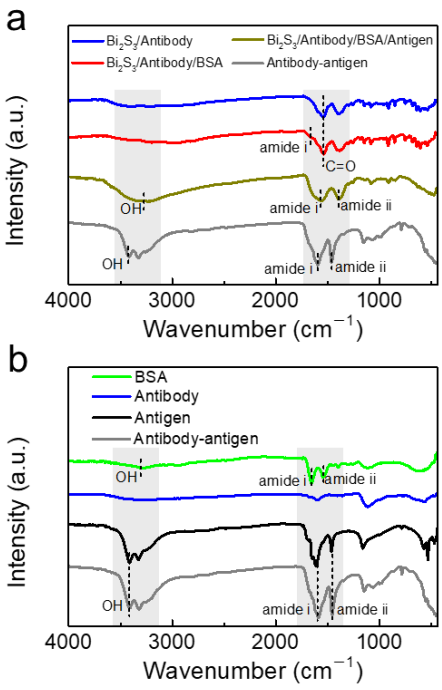

Figure 4. (**a**) FTIR spectra of Bi_2S_3/Antibody, Bi_2S_3/Antibody/BSA, Bi_2S_3/Antibody/BSA/Antigen, and Antibody-antigen complex; and (**b**) the FTIR spectra of BSA, Antibody, Antigen, and Antibody-antigen complex.

3.3. Electrochemical Measurement of Cytokeratin 18 Antigen Protein

The standard CK18 antigen protein solutions (1 pg mL^{-1}) in PBS with pH ranging from 5 to 9 were prepared to explore the effect of the pH on the recorded current signal (Figure S2). Here, we extracted the peak currents and defined the ΔI as ($I_{PBS} - I_{Antigen}$), where I_{PBS} and $I_{Antigen}$ represented the peak current measured in pure PBS solution and antigen solution, respectively. The highest current signal for CK18 antigen was obtained in PBS solutions, pH 7; hence, this medium was used in the following studies. The sensing performance for recombinant human CK18 antigen protein testing was analyzed by DPV and EIS measurements. The standard antigen protein solutions in PBS with concentrations ranging from 1 pg mL^{-1} to 10 ng mL^{-1} were prepared to explore the relationship between the concentration of determinand and the output electrical signals. Figure 5a shows the DPV curves measured at different antigen concentrations. The peak currents at DPV mode decreased linearly with the increase of antigen concentration. Here, we extracted the peak currents and defined the response as $I_{PBS}/I_{Antigen}$. The response signal showed an S-shaped curve response (logarithmic fitting relationship) with increasing CK18 antigen concentration (Figure 5b), which reflected the kinetic processes of immune reaction between CK18 antigen and antibody [35]. The reaction rate was slow initially, and then accelerated with the increase of concentration, finally reaching the saturation state gradually. The response curve corresponds to the process of antigen/antibody interaction, including molecular recognition and reaction. Molecular interactions generally involve molecular bonding and equilibrium. Through the fitting of the least-square method (1 pg mL^{-1} to 1 ng mL^{-1}), the slope of antigen concentration-response curve was obtained. Furthermore, the biosensor exhibited wide linear dynamic range (1–1000 pg mL^{-1}). The relative standard deviation of blank value measured in PBS solution was defined as SD_{blank}. According to the formula ($3SD_{blank}$/slope), the limit-of-detection (LOD) of the biosensor for recombinant human cytokeratin 18 protein testing was estimated to be 39 fg mL^{-1} (1.87 fM (fmol L^{-1})). Biomarkers with different concentration ranges correspond to different therapeutic targets, hence regulating the physiological activity of targets can effectively improve disease symptoms. Further, the identification of disease-specific target molecules is the basis of modern drug development. The accurate detection of different concentrations of bladder cancer biomarkers is conducive to the follow-up rational grading diagnosis and treatment, and quickly assist doctors to diagnose patients.

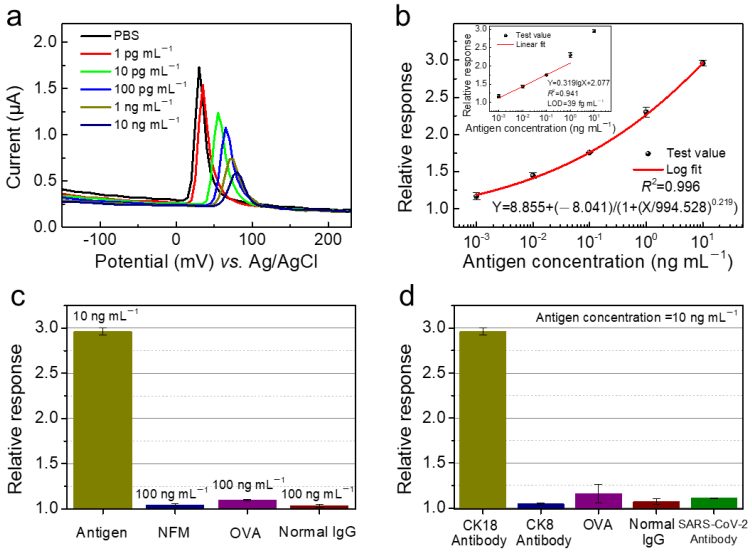

Figure 5. (**a**) The DPV voltamograms corresponding to increasing CK18 antigen concentrations (0 to 10 ng mL^{-1}); and (**b**) antigen concentration-dependent response curve using logistic fit and linear fit. (**c**) The selectivity against NFM, OVA, and normal IgG. (**d**) The selectivity of the biosensor with CK8 antibody protein, OVA, normal IgG, and SARS-CoV-2 antibody immobilization.

Owing to the complex composition of actual biological samples, the specificity of the biosensor is crucial to the accuracy of detection results. Here, non-fat milk (NFM), ovalbumin (OVA), and human normal immunoglobulin (normal IgG) were selected to evaluate the specificity of electrochemical biosensor employing Bi_2S_3 NCs-modified electrode. As shown in Figure 5c, the response toward the above three proteins were rather low compared to CK18 antigen protein. The electrical labelling of CK18 antibody protein based on Bi_2S_3 NCs plays a key role in improving the sensitivity and specificity of the biosensor. To further verify the selectivity of the biosensor, several proteins including CK8 antibody protein, OVA, normal IgG, and SARS-CoV-2 antibody were selected to be immobilized on the surface of the NCs film for device modification, and CK18 antigen was used as the target for testing. The responses of the above four proteins-immobilized biosensors were less than 1.25, which were rather low compared to the response of the biosensor with CK18 antibody protein-immobilization (Figure 5d). Biologically active molecules (biomolecules) anchored to sensing materials are critical for antigen-antibody specific binding reaction. Unpaired biomolecules would not produce significant current signals. The results indicated the effectiveness of NCs as the electronic labelling of CK18 antibody protein in contributing sensitive and specific signal. As shown in Table 1, compared with the reported literatures on bladder cancer biomarker detection [17,23,36–38], this work demonstrated that the electrochemical sensor had fast response, low LOD and wide linear dynamic range.

Table 1. Parameters comparison for the detection of bladder cancer biomarkers.

Biomarkers	Response Time	LOD	Linear Range	Ref.
CK19	-	1 ng mL^{-1}	1–100 ng mL^{-1}	[17]
CK8	-	1 ag mL^{-1}	0.001–100 fg mL^{-1}	[23]
NMP22	~1 min	0.33 pg mL^{-1}	0.001–20 ng mL^{-1}	[36]
NMP22	~1 min	0.1 pg mL^{-1}	1–500 pg mL^{-1}	[37]
NMP22	~1 min	3.3 pg mL^{-1}	0.01–18 ng mL^{-1}	[38]
CK18	~30 s	39 fg mL^{-1}	1–1000 pg mL^{-1}	Ours

3.4. The Sensing Mechanism of the Electrochemical Biosensor

EIS provides quantitative electrical parameters for the equivalent circuit model of the electrochemical system. We further tested the EIS curves of the biosensor in PBS and in various concentrations of CK18 antigen protein solutions (1 pg mL^{-1} to 10 ng mL^{-1}). According to the equivalent circuit model of electrochemical three-electrode (Figure 6a), fitted EIS curves were displayed in Figure 6b. The equivalent circuit was comprised of R_s, C, R_1, Q, R_{ct}, and Z_w. Here, R_1, C, R_{ct}, and Q represent the solution resistance, film capacitance, the charge transfer resistance, and the capacitance of the electrical double layer located at the electrode-electrolyte interface. With the increase of CK18 antigen concentration, the antibody and antigen specific binding reactions located at the electrode–electrolyte interface were more active, causing the change of modification layer on the WE, which may lead to the slight increase initially and subsequent decrease of R_1 (Figure 6c) [39]. When the CK18 antigen was added to the reaction system, the value of C decreased, but remained relatively stable with the increase of CK18 antigen concentration. protein concentration in the solution system increased, resulting in the increase of solution resistance R_S. R_{ct} reflects the resistance of the charge transfer across the fluid–solid interface, the value of R_{ct} increased sharply initially and then showed the trend of slight decrease with the increase of CK18 antigen concentration (Figure 6d). The value of Q tended to decrease with the increase of CK18 antigen concentration.

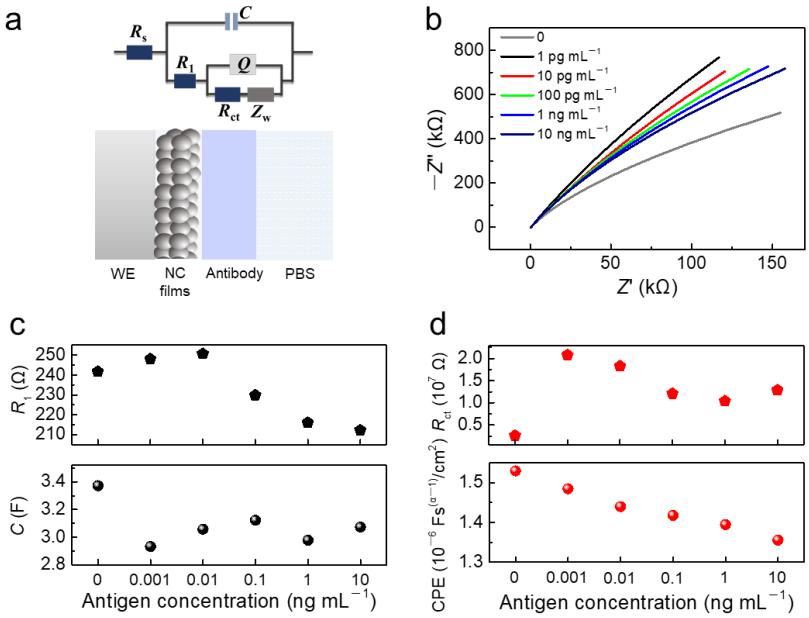

Figure 6. (**a**) The equivalent circuit model of Bi_2S_3 NCs-modified electrode; (**b**) EIS characterizations of C/CQDs/Antibody/BSA electrodes in PBS and antigen solutions with different concentrations (1 pg mL^{-1} to 10 ng mL^{-1}); (**c**) the value of R_1 and C in PBS and antigen solutions with different concentrations (1 pg mL^{-1} to 10 ng mL^{-1}); and (**d**) the value of R_{ct} and CPE in PBS and antigen solutions with different concentrations (1 pg mL^{-1} to 10 ng mL^{-1}).

4. Conclusions

In this work, bismuth sulfide (Bi_2S_3) semiconductor nanocrystals (NCs) were used as the modification materials to construct the planar electrochemical biosensor, and the specific recognition and efficient signal transduction of biological proteins as the biomarker of bladder cancer were achieved by the design of a NCs–protein interface. The electrochemical biosensor employing Bi_2S_3 NCs-modified electrode exhibited the sensing performance of cytokeratin 18 antigen protein with the detection time of less than 30 s, the limit of detection (LOD) of 1.87 fM (fmol L^{-1}), and wide linear dynamic range (1–1000 pg mL^{-1}), which demonstrated rapidity, high sensitivity, convenient use, and non-invasive detection. It can provide immunological evidence for early diagnosis, recurrence monitoring, and prognosis of bladder cancer, which shows the application prospect in the field of disease biomarkers diagnosis, epidemiological investigation, and physiological parameters monitoring. The green bismuth sulfide nanocrystals were developed, and the physical and chemical properties could be designed by adjusting the size, morphology, and composition to adapt to different biomolecules. The semiconductor nanocrystals immunoassay method developed here is expected to promote the development of low-cost clinical detecting instrument, POCT, wearable physiological monitoring, and home self-inspection.

Supplementary Materials: The following supporting information can be downloaded at: https://www.mdpi.com/article/10.3390/chemosensors10020048/s1, Figure S1: CV characterizations obtained for $[Fe(CN)_6]^{3-}/^{4-}$ on the bare (a) and modified sensors (b) at the different scan rates within the range 25–200 mV s^{-1}. the corresponding I_p vs. $v^{1/2}$ plot for bare (c) and modified sensors (d); Figure S2: The effect of the pH on the recorded current signal.

Author Contributions: Conceptualization, H.L. (Huageng Liang) and H.L. (Huan Liu); methodology, H.L. (Huan Liu); software, Y.Z.; formal analysis, Y.Z. and Y.T.; investigation, Y.Z., Y.T., Q.H., J.H., J.K., R.G. and P.Z.; resources, H.L. (Huan Liu); data curation, Y.Z. and Y.T.; writing—original draft preparation, Y.Z. and Y.T.; writing—review and editing, H.L. (Huageng Liang) and H.L. (Huan Liu); supervision, H.-Y.L., H.L. (Huageng Liang) and H.L. (Huan Liu); funding acquisition, H.L. (Huageng Liang) and H.L. (Huan Liu). All authors have read and agreed to the published version of the manuscript.

Funding: This work was supported by National Natural Science Foundation of China (No. 61922032). We thank the Program for HUST Academic Frontier Youth Team (2018QYTD06) and Innovation Fund of WNLO (Wuhan National Laboratory for Optoelectronics) for equipment support.

Institutional Review Board Statement: Not applicable.

Informed Consent Statement: Not applicable.

Data Availability Statement: Not applicable.

Acknowledgments: We thank the Analytical and Testing Center of HUST for the characterization support.

Conflicts of Interest: All authors have given their approval for the final version of the manuscript and declare no competing financial interests.

References

1. Burger, M.; Catto, J.W.F.; Dalbagni, G.; Grossman, H.B.; Herr, H.; Karakiewicz, P.; Kassouf, W.; Kiemeney, L.A.; La Vec-chia, C.; Shariat, S.; et al. Epidemiology and Risk Factors of Urothelial Bladder Cancer. *Eur. Urol.* **2013**, *63*, 234–241. [CrossRef] [PubMed]
2. Donato, F.; Boffetta, P.; Fazioli, R.; Aulenti, V.; Porru, G.S. Bladder cancer, tobacco smoking, coffee and alcohol drinking in Brescia, northern Italy. *Eur. J. Haematol.* **1997**, *13*, 795–800.
3. Kaufman, D.S.; Shipley, W.U.; Feldman, A.S. Bladder cancer. *Lancet* **2009**, *374*, 239–249. [CrossRef]
4. Schmidbauer, J.; Witjes, F.; Schmeller, N.; Donat, R.; Susani, M.; Marberger, M. Improved detection of urothelial carcinoma in situ with hexaminolevulinate fluorescence cystoscopy. *J. Urol.* **2004**, *171*, 135–138. [CrossRef] [PubMed]
5. Grossman, H.B.; Gomella, L.; Fradet, Y.; Morales, A.; Presti, J.; Ritenour, C.; Nseyo, U.; Droller, M.J.; PC B302/01 Study Group. A phase iii, multicenter comparison of hexaminolevulinate fluorescence cystoscopy and white light cystoscopy for the detection of superficial papillary lesions in patients with bladder cancer. *J. Urol.* **2007**, *178*, 62–67. [CrossRef] [PubMed]
6. Matsumoto, K.; Irie, A.; Satoh, T.; Kuruma, H.; Baba, S. Occupational bladder cancer: From cohort study to biologic molecular marker. *Med. Sci. Monit.* **2005**, *11*, RA311–RA315. [PubMed]
7. Jordan, B.; Meeks, J.J. T1 bladder cancer: Current considerations for diagnosis and management. *Nat. Rev. Urol.* **2019**, *16*, 23–34. [CrossRef]
8. Eissa, S.; Swellam, M.; Amin, A.; Balbaa, M.E.; Yacout, G.A.; El-Zayat, T.M. The clinical relevance of urine-based markers for diagnosis of bladder cancer. *Med. Oncol.* **2011**, *28*, 513–518. [CrossRef]
9. Meo, A.D.; Bartlett, J.; Cheng, Y.; Pasic, M.D.; Yousef, G.M. Liquid biopsy: A step forward towards precision medicine in urologic malignancies. *Mol. Cancer* **2017**, *16*, 80. [CrossRef]
10. Schroeder, G.L.; Lorenzo-Gomez, M.F.; Hautmann, S.H.; Friedrich, M.G.; Ekici, S.; Huland, H.; Lokeshwar, V. A side by side comparison of cytology and biomarker for bladder cancer detection. *J. Urol.* **2004**, *172*, 1123–1126. [CrossRef]
11. Christoph, F.; Weikert, S.; Wolff, I.; Schostak, M.; Tabiti, K.; Müller, M.; Schrader, M. Urinary cytokeratin 20 mRNA expression has the potential to predict recurrence in superficial transitional cell carcinoma of the bladder. *Cancer Lett.* **2007**, *245*, 121–126. [CrossRef]
12. Li, Y.P.; Jia, X.P.; Jiang, Y.Q.; Wang, W.; Wang, Y.L.; Wang, X.L.; Guo, Y.X. Differential expression of cytokeratin 14 and 18 in bladder cancer tumorigenesis. *Exp. Biol. Med.* **2018**, *243*, 344–349. [CrossRef]
13. Gaston, K.E.; Grossman, H.B. Proteomic assays for the detection of urothelial cancer. *Methods Mol. Biol.* **2010**, *641*, 303–323.
14. Wang, J.; Zhang, J.; Li, T.; Shen, R.; Li, G.; Ling, L. Strand displacement amplification-coupled dynamic light scattering method to detect urinary telomerase for non-invasive detection of bladder cancer. *Biosens. Bioelectron.* **2019**, *131*, 143–148. [CrossRef]
15. Arya, S.K.; Estrela, P. Electrochemical ELISA-based platform for bladder cancer protein biomarker detection in urine. *Biosens. Bioelectron.* **2018**, *117*, 620–627. [CrossRef]
16. Dar, V.S.; Ghosh, S.; Broor, S. Rapid detection of rotavirus by using colloidal gold particles labeled with monoclonal antibody. *J. Virol. Methods* **1994**, *47*, 51–58. [CrossRef]
17. Lei, Q.F.; Zhao, L.L.; Ye, S.X.; Sun, Y.; Xie, F.J.; Zhang, H.; Zhou, F.J.; Wu, S. Rapid and quantitative detection of urinary cyfra21-1 using fluorescent nanosphere-based immunochromatographic test strip for diagnosis and prognostic monitoring of bladder cancer. *Artif. Cell. Nanomed. Biotechnol.* **2019**, *47*, 4266–4272. [CrossRef]
18. Xu, S.; Dong, B.; Zhou, D.L.; Yin, Z.; Cui, S.B.; Xu, W.; Chen, B.J.; Song, H.W. Paper-based upconversion fluorescence resonance energy transfer biosensor for sensitive detection of multiple cancer biomarkers. *Sci. Rep.* **2016**, *6*, 23406. [CrossRef]
19. Azzouz, A.; Hejji, L.; Kim, K.-H.; Kukkar, D.; Souhail, B.; Bhardwaj, N.; Brown, R.; Zhang, W. Advances in surface plasmon resonance–based biosensor technologies for cancer biomarker detection. *Biosens. Bioelectron.* **2022**, *197*, 113767. [CrossRef]
20. Munge, B.S.; Coffey, A.L.; Doucette, J.M.; Somba, B.K.; Malhotra, R.; Patel, V.; Gutkind, J.S.; Rusling, J.F. Nanostructured immunosensor for attomolar detection of cancer biomarker interleukin-8 using massively labeled superparamagnetic particles. *Angew. Chem. Int. Ed.* **2011**, *50*, 7915–7918. [CrossRef]
21. Ricci, F.; Volpe, G.; Micheli, L.; Palleschi, G. A review on novel developments and applications of immunosensors in food analysis. *Anal. Chim. Acta* **2007**, *605*, 111–129. [CrossRef] [PubMed]

22. Sadik, O.A.; Emon, J. Applications of electrochemical immunosensors to environmental monitoring. *Biosens. Bioelectron.* **1996**, *11*, i–x. [CrossRef]
23. Yang, Y.; Zeng, B.; Li, Y.; Liang, H.; Yuan, Q. Construction of MoS2 field effect transistor sensor array for the detection of bladder cancer biomarkers. *Sci. China Chem.* **2020**, *63*, 997–1003. [CrossRef]
24. Liu, H.; Li, M.; Voznyy, O.; Hu, L.; Fu, Q.Y.; Zhou, D.X.; Xia, Z.; Sargent, E.H.; Tang, J. Physically flexible, rapid-response gas sensor based on colloidal quantum dot solids. *Adv. Mater.* **2014**, *26*, 2718–2724. [CrossRef] [PubMed]
25. Tang, J.; Sargent, E.H. Colloidal-quantum-dot photovoltaics using atomic-ligand passivation. *Nat. Mater.* **2011**, *10*, 765–771. [CrossRef] [PubMed]
26. Zhu, Z.J.; Yeh, Y.C.; Tang, R.; Yan, B.; Tamayo, J.; Vachet, R.W.; Rotello, V.M. Stability of quantum dots in live cells. *Nat. Chem.* **2011**, *3*, 963–968. [CrossRef] [PubMed]
27. Yu, H.W.; Lee, J.; Kim, S.; Nguyen, G.H.; Kim, I.S. Electrochemical immunoassay using quantum dot/antibody probe for identification of cyanobacterial hepatotoxin microcystin-LR. *Anal. Bioanal. Chem.* **2009**, *394*, 2173–2181. [CrossRef]
28. Kan, H.; Li, M.; Song, Z.L.; Liu, S.S.; Zhang, B.H.; Liu, J.Y.; Li, M.Y.; Zhang, G.Z.; Jiang, S.L.; Liu, H. Highly sensitive response of solution-processed bismuth sulfide nanobelts for room-temperature nitrogen dioxide detection. *J. Colloid Interf. Sci.* **2017**, *506*, 102–110. [CrossRef]
29. Rudnicki, K.; Brycht, M.; Leniart, A.; Domagała, S.; Kaczmarek, K.; Kalcher, K.; Skrzypek, S. A sensitive sensor based on single-walled carbon nanotubes: Its preparation, characterization and application in the electrochemical determination of drug clorsulon in milk samples. *Electroanalysis* **2020**, *32*, 375–383. [CrossRef]
30. Chen, X.J.; Wang, Y.Y.; Zhou, J.J.; Yan, W.; Li, X.H.; Zhu, J.J. Electrochemical impedance immunosensor based on three-dimensionally ordered macroporous gold film. *Anal. Chem.* **2020**, *80*, 2133–2140. [CrossRef]
31. Qu, C.L.; Li, H.; Zhou, S.; Li, G.D.; Wang, C.; Snyders, R.; Bittencourt, C.; Li, W.J. Bi2S3/rGO Composite Based Electrochemical Sensor for Ascorbic Acid Detection. *Chemosensors* **2021**, *9*, 190. [CrossRef]
32. Cademartiri, L.; Scotognella, F.; O'Brien, P.G.; Lotsch, B.V.; Thomson, J.; Petrov, S.; Kheran, N.P.; Ozin, G.A. Cross-linking Bi2S3 ultrathin nanowires: A platform for nanostructure formation and biomolecule detection. *Nano Lett.* **2009**, *9*, 1482–1486. [CrossRef]
33. Bandekar, J. Amide modes and protein conformation. *BBA-Proteins Proteom.* **1992**, *1120*, 123–143. [CrossRef]
34. Wang, Q.S.; Ye, F.Y.; Fang, T.T.; Niu, W.H.; Liu, P.; Min, X.M.; Li, X. Bovine serum albumin-directed synthesis of biocompatible CdSe quantum dots and bacteria labeling. *J. Colloid Interf. Sci.* **2011**, *355*, 9–14. [CrossRef]
35. Dudley, R.A.; Edwards, P.; Ekins, R.P.; Finney, D.J.; Mckenzie, I.G.; Raab, G.M.; Rodbard, D.; Rodgers, R.P. Guidelines for immunoassay data processing. *Clin. Chem.* **1985**, *8*, 1264–1271. [CrossRef]
36. Wu, D.; Wang, Y.G.; Zhang, Y.; Ma, H.M.; Yan, T.; Du, B.; Wei, Q. Sensitive electrochemical immunosensor for detection of nuclear matrix protein-22 based on NH2-SAPO-34 Supported Pd/Co Nanoparticles. *Sci. Rep.* **2016**, *6*, 24551. [CrossRef]
37. Lee, M.-H.; Thomas, J.; Chang, Y.-C.; Tsai, Y.-S.; Liu, B.-D.; Lin, H.-Y. Electrochemical sensing of nuclear matrix protein 22 in urine with molecularly imprinted poly(ethylene-co-vinyl alcohol) coated zinc oxide nanorod arrays for clinical studies of bladder cancer diagnosis. *Biosens. Bioelectron.* **2016**, *79*, 789–795. [CrossRef]
38. Li, N.; Wang, Y.L.; Li, Y.Y.; Cao, W.; Ma, H.M.; Wu, D.; Du, B.; Wei, Q. A label-free electrochemical immunosensor based on Au@Pd/Ag yolk-bimetallic shell nanoparticles and amination graphene for detection of nuclear matrix protein 22. *Sens. Actat.-B Chem.* **2014**, *202*, 789–795. [CrossRef]
39. Zhao, Y.N.; Chen, J.J.; Hu, Z.X.; Chen, Y.; Tao, Y.B.; Wang, L.; Li, L.; Wang, P.; Li, H.-Y.; Zhang, J.B.; et al. All-solid-state SARS-CoV-2 protein biosensor employing colloidal quantum dots-modified electrode. *Biosens. Bioelectron.* **2022**, *202*, 113974. [CrossRef]